JMJD3 is Involved in Intracranial Aneurysm Development by Regulating DLX2 Expression through H3K27me3 Modification

Xuan Wang,[1] Nan Li[2] and Tong Li[3]

[1]Department of Clinical Laboratory, Laohekou No.1 Hospital, Xiangyang, Hubei, China
[2]Department of Pharmacy, Xiangyang Central Hospital, Affiliated Hospital of Hubei University of Arts and Science, Xiangyang, Hubei, China
[3]Department of Neurology, Xiangyang Central Hospital, Affiliated Hospital of Hubei University of Arts and Science, Xiangyang, Hubei, China

Intracranial aneurysms are dilatations in the arteries that supply blood to the brain. Rupture of an intracranial aneurysm leads to a subarachnoid hemorrhage, which is fatal in about 50% of the cases. Microarray-based mRNA expression studies provide unbiased information about molecular mechanisms of intracranial aneurysm and the foundation for functional studies. In this study, by using a Gene Expression Omnibus (GEO) dataset, we identified distal-less homeobox 2 (DLX2) as a significantly upregulated gene in intracranial aneurysms and set to dissect its functional role and upstream mechanism. Here, we found that DLX2 expression was elevated in intracranial aneurysm patients. Silencing of DLX2 suppressed the proliferative capacity of human aortic vascular smooth muscle cells (HA-VSMC) and promoted their apoptosis. Moreover, loss of DLX2 promoted collagen I and collagen III and inhibited the levels of MMP2/9 and pro-inflammatory factors. Additionally, jumonji domain-containing protein 3 demethylase (JMJD3) promoted DLX2 expression by inhibiting H3K27me3 modification. Depletion of JMJD3 exerted the same function as DLX2 *in vitro* and *in vivo*, whereas overexpression of DLX2 in the presence of JMJD3 knockdown led to accentuated intracranial aneurysm progression and enhanced HA-VSMC survival. We conclude that JMJD3 promotes DLX2 expression through inhibition of H3K27me3 modification, thereby promoting intracranial aneurysm formation.

Introduction

Intracranial aneurysms, also called cerebral aneurysms, are dilatations in the arteries that supply blood to the brain (Tromp et al. 2014). The most devastating consequence of intracranial aneurysm rupture is aneurysmal subarachnoid hemorrhage, with an impact ranging from mild symptoms to severe disability or mortality (Samuel and Radovanovic 2019). Although surgical clipping and endovascular therapy have been the major therapeutic methods for intracranial aneurysm, potentially serious complications related to those invasive procedures should not be overlooked (Liu et al. 2019). Understanding the mechanisms underlying the formation and progression intracranial aneurysm helps us to search for possible therapeutic strategies,

particularly safe and effective non-invasive therapies.

In the present study, we used the Gene Expression Omnibus (GEO) database to filter key genes in intracranial aneurysm. Distal-less homeobox 2 (*DLX2*) was found to be one of the most significantly expressed genes in intracranial aneurysm. The DLX genes are among the key transcription factors involved in regulating the development of craniofacial structures in vertebrates (Tan and Testa 2021). *DLX2* has been revealed to be upregulated in thoracic aortic aneurysms (Jones et al. 2008). However, there is little information regarding its role in intracranial aneurysm. Recently, epigenetics has become a new research hotspot in intracranial aneurysm (Poppenberg et al. 2021). Epigenetics, defined as transcriptional memory which alters gene expression without changing the genome can be distinguished into

three kinds, histone modifications, DNA methylation and non-coding RNAs (Zurek et al. 2021). For instance, inhibition of histone deacetylase 9 upregulated microRNA-92a to repress the progression of intracranial aneurysm (Cai et al. 2021). Therefore, we set to decipher the upstream epigenetic modifier of *DLX2* in intracranial aneurysm. Interestingly, inhibition of jumonji domain-containing protein 3 demethylase (JMJD3, also termed KDM6B) has been reported to protect against abdominal aortic aneurysms (Davis et al. 2021). As a consequence, we wondered whether it exerted the same function in intracranial aneurysm as well. JMJD3 is a histone demethylase that specifically removes methyl groups from tri-methylation of lysine from histone 3 (H3K27me3), a repressive epigenetic mark (Lagunas-Rangel 2021; Sanchez et al. 2021). JMJD3 promoted the development of esophageal squamous cell carcinoma through epigenetic activation of MYC (Li et al. 2020). We aimed to probe the role of the JMJD3/*DLX2* axis in intracranial aneurysm development. Vascular smooth muscle cells (VSMC) can alter their phenotype from one primarily concerned with contraction to a pro-inflammatory and matrix remodeling phenotype upon environmental stimulation, which highlighted a critical process behind the peripheral vascular disease and atherosclerosis, a key element of the pathology of intracranial aneurysm (Starke et al. 2014). Therefore, we speculated that JMJD3 may mediate *DLX2* via the H3K27me3 modification, thus modulating intracranial aneurysm progression by controlling the phenotype of VSMC.

Materials and Methods

Participants and tissue samples

Written informed consent was acquired from all patients before this study. The protocol of this study was confirmed by the Ethic Committee of Laohekou No.1 Hospital and based on the ethical principles for medical research involving human subjects of *the Helsinki Declaration.* Patients with intracranial aneurysm who underwent surgery from July 2018 to June 2021 were selected for this study [9 males and 7 females, aged 30-75 years, mean age 51.12 ± 9.32 years, mean ± standard deviation (SD)], and all cases were diagnosed by digital subtraction angiography. Sixteen normal samples were collected from volunteers with traumatic brain injury (8 males and 8 females, aged 31-73 years, mean age 53.42 ± 8.45 years). Excised tissues were immediately frozen in liquid nitrogen and stored at $-80°C$.

Cell culture and cell transfection

Human aortic-VSMC (HA-VSMC) were purchased from Procell (CP-H116, Wuhan, Hubei, China) and cultured in Dulbecco's modified Eagle's medium (11965092, Gibco, Carlsbad, CA, USA) containing 10% fetal bovine serum (10099141C, Thermo Fisher Scientific Inc., Waltham, MA, USA) and 1% penicillin/streptomycin (15140122, Gibco) at $37°C$ in a 5% CO_2 incubator.

The cells were transfected with: short hairpin RNA (shRNA) targeting negative control (sh-NC), short hairpin RNA (shRNA) targeting DLX2-1 (sh-DLX2-1), sh-DLX2-2, sh-DLX2-3, sh-JMJD3-1, sh-JMJD3-2, sh-JMJD3-3, sh-JMJD3 + overexpression vector (oe)-NC, or sh-JMJD3 + oe-DLX2. The sequence of the shRNA (stem-loop sequence is CTCGAG) is as follows: sh-DLX2-1: AGGACCTTGAGCCTGAAATTCCTCGAG GAATTTCAGGCTCAAGGTCCT; sh-DLX2-2: TGAGA GCAGAGACCACTTATCCTCGAGGATAAGTGG TCTCTGCTCTCA; sh-DLX2-3: CGCACCATCTACTCCA GTTTCCTCGAGGAAACTGGAGTAGATGGTGCG; sh-JMJD3-1: AGTCCCACTCACCTCTATTTACTCGAGT AAATAGAGGTGAGTGGGACT; sh-JMJD3-2: GATCTC TATGCATCCAATATTCTCGAGAATATTGGATGC ATAGAGATC; sh-JMJD3-3: GGAGACCTCGTGTGGATT AATCTCGAGATTAATCCACACGAGGTCTCC.

The day before transfection, HA-VSMC at the logarithmic growth phase were seeded in 12-well cell culture plates at a concentration of 1×10^5 cells/mL. When the cell confluence reached 50%-70%, well-containing cells were added with 800 μL of serum-free medium, the above vectors, and Lipofectamine™ 2000 mixture (11668027, Thermo Fisher Scientific). The cells were cultured for 6 h, and the culture medium was renewed with fresh media. The cells were collected 48 h after transfection, and RNA and protein were extracted for subsequent experiments.

Operative procedure

This animal protocol was approved by the Institutional Animal Care and Use Committee of Laohekou No.1 Hospital, and all animals were treated and cared for following the NIH's 1996 guidelines for the care and use of laboratory animals. Fifty-six healthy adult male Sprague-Dawley rats (6 weeks old, weighing 200-240 g) were purchased from Hunan SJA Laboratory Animal Co., Ltd. (Changsha, Hunan, China). All rats were housed on a 12/12 h light/dark cycle with *ad libitum* access to chow and drinking water.

After general anesthesia with intraperitoneal injection of 50 mg/kg pentobarbital, the rats were shaved. The dorsal left subcostal margin was cut with a longitudinal incision of approximately 1.5-2 cm. The thumb was placed on the dorsum of the rat, and the index and middle fingers were on the belly of the rat. The kidney was pushed out of the incision with the index finger to expose the kidney and the dorsum of the renal pedicle. The posterior branch of the renal artery can be seen under 2.5 × magnification. The posterior branch of the renal artery was separated from the vein automatically due to tension at the medial incision with forceps and ligated with 0/3 silk. At this point, the mid to upper portion of the posterior renal segment showed a distinctly mapped ischemic zone due to blockage of the posterior branch of the renal artery. The kidney was put back into the abdominal cavity, and the skin was sutured. The skin, subcutaneous, and broad cervical muscles were incised in the

anterior mid-neck area (2 cm long). The left common carotid artery was separated from the vagus nerve and ligated with a 4# silk suture, and the incision was intermittently sutured.

Eight rats were selected as the sham group and underwent the same surgery as the experimental group, but were not treated with ligation. The remaining 48 rats were subjected to ligation of the left common carotid artery and the posterior branch of the left renal artery. After 48 h, 40 successfully modeled intracranial aneurysm rats were further intraperitoneally injected with 1 mL lentiviral vector (1 × 10^8 PFU/mL) harboring short hairpin RNA (shRNA) targeting negative control (sh-NC), sh-JMJD3 (the sequence of sh-JMJD3-1 as described above), sh-DLX2, sh-JMJD3 + overexpression vector (oe)-NC, and sh-JMJD3 + oe-DLX2. Blood pressure was measured at 0, 7, and 28 days. Systolic blood pressure was measured by a non-invasive blood pressure meter (Shanghai Yuyan Instruments Co., Ltd., Shanghai, China). The rats were euthanized after 4 weeks for tissue sampling and tail vein blood collection.

Hematoxylin-eosin (HE) staining

Rat aneurysm tissues were fixed in 10% neutral formalin solution for 24 h, dehydrated in gradient alcohol, and cleared in xylene, and paraffin-embedded. The embedded tissue blocks were trimmed and sectioned. Then, the sections were cleared with xylene, hydrated with gradient alcohol, washed under distilled water for 1 min, and stained with hematoxylin for 3 min, treated with 0.5% hydrochloric acid alcohol fractionation solution for 10 s, and stained with eosin for 5 min. After conventional dehydration, clearing, and sealing, the sections were observed with a microscope (Leica-DM2500, Leica Microsystems GmbH, Wetzlar, Germany).

Enzyme-linked immunosorbent assay (ELISA)

Blood from the tail vein of rats was centrifuged, and the supernatant was assayed for the inflammatory factors, tumor necrosis factor-α (TNF-α), interleukin (IL)-6, and IL-1β according to the instructions of the TNF-α (ab236712, Abcam, Cambridge, UK), IL-6 (ab234570, Abcam) and IL-1β (ab255730, Abcam). The optical density (OD) value was read at 450 nm using an ELISA reader (BioTek Instruments, Winooski, VT, USA).

RNA isolation and reverse transcription-quantitative PCR (RT-qPCR) analysis

Total tissue or cellular RNA was extracted using TRIzol (Thermo Fisher Scientific), and cDNA was obtained by reverse transcription using a reverse transcription kit (RR047A, Takara Biotechnology Ltd., Dalian, Liaoning, China). RT-qPCR was performed according to the SYBR® Premix Ex TaqTM II kit (RR820A, Takara) instructions. The primers were synthesized by Shanghai Sangon Biological Engineering Technology & Services Co., Ltd. (Shanghai, China) (Table 1). GAPDH served as an internal

Table 1. Oligonucleotide primer sequences for reverse transcription-quantitative PCR (RT-qPCR).

Gene	Sequence
JMJD3	F 5'-AAGGACGAGCCAGCCTACTA-3'
	R 5'-GGGCTCAGGGAAAGGCG-3'
DLX2	F 5'-GGCCTCAACAACGTCCCTTA-3'
	R 5'-CTTTTGGAAACGCCGCTGAA-3'
GAPDH	F 5'-AATGGGCAGCCGTTAGGAAA-3'
	R 5'-GCGCCCAATACGACCAAATC-3'
DLX2 promoter (Human)	F 5'-AGCAACAGCCAATCAGAAGC-3'
	R 5'-CAAAACGCCAGTCTGTCTCC-3'

F, forward; R, reverse; DLX2, distal-less homeobox 2; JMJD3, jumonji domain-containing protein 3; GAPDH, glyceraldehyde-3-phosphate dehydrogenase.

control for mRNA. All the samples were normalized to internal controls, and fold changes were calculated by the $2^{-\Delta\Delta Ct}$ method via relative quantification.

Western blot

Total protein in tissues and cells was extracted using the radio-immunoprecipitation assay kit (R0010, Beijing Solarbio Life Sciences Co., Ltd., Beijing, China), incubated on ice for 30 min, and centrifuged at 4°C for 10 min at $8,000 \times g$. Protein concentration was determined using the Pierce™ BCA Protein Quantification Kit (23225, Thermo Fisher Scientific). Each sample was extracted with 50 μg of protein, fractionated on a 10% sodium dodecyl sulfate-polyacrylamide gel, and transferred onto polyvinylidene fluoride membranes. The membranes were blocked at room temperature with Tris-buffered saline-Tween 20 containing 5% bovine serum albumin (BSA) and incubated with diluted primary antibodies against rabbit antibodies to DLX2 (ab272902, Abcam), JMJD3 (ab169197, Abcam), collagen type I alpha 1 chain (COL1A1) (#91144, Cell Signaling Technologies, Beverly, MA, USA), collagen type III alpha 1 chain (COL3A1) (sc-271249, Santa Cruz Biotechnology Inc., Santa Cruz, CA, USA), matrix metalloproteinase-2 (MMP-2) (ab181286, Abcam), matrix metalloproteinase-9 (MMP9) (ab76003, Abcam), H3K27me3 (#9733, Cell Signaling Technologies), and GAPDH (ab9485, Abcam) overnight at 4°C and with the secondary antibody goat anti-rabbit IgG antibody (ab6721, Abcam) or rabbit anti-mouse IgG antibody (ab6728, Abcam) at room temperature. Bands were developed using Pierce™ ECL Fluorescence Detection Kit (32209, Thermo Fisher Scientific). The gel image analysis software Image J was used to analyze the gray value of each band and calculate the gray value ratio of the target protein to the internal control protein band.

Cell proliferation assay

The cells to be tested were seeded in 24-well plates, and EdU (C10310-1, Guangzhou RiboBio Co., Ltd.,

Guangzhou, Guangdong, China) was added for a 2-h incubation. The cells were fixed with phosphate-buffered saline (PBS) containing 4% paraformaldehyde solution at room temperature for 15 min, washed twice with PBS containing 3% BSA, incubated with PBS containing 0.5% Triton-100 at room temperature for 20 min, and then washed twice with PBS containing 3% BSA. The cells were then stained with 100 μL EdU solution for 30 min at room temperature in the dark, and 4',6-Diamidino-2-Phenylindole was used to stain nuclei for 5 min. After sealing, 6-10 fields of view were randomly observed, and the number of positive cells in each field of view was recorded. EdU labeling rate (%) = number of positive cells/(number of positive cells + number of negative cells) × 100%.

Cell apoptosis analysis

After 48 h of transfection, the cells were detached with ethylenediaminetetraacetic acid-free trypsin (Thermo Fisher Scientific) and centrifuged two times at 3,000 r/min for 30 min and 15 min, respectively. Annexin-V-fluorescein isothiocyanate (FITC)/propidium iodide (PI) staining solution was prepared using N-2-Hydroxyethylpiperazine-N'-2-Ethanesulfonic acid (HEPES), Annexin V-FITC and PI at 50:1:2 according to the Annexin-V-FITC Apoptosis Detection Kit (APOAF, Sigma-Aldrich Chemical Company, St. Louis, MO, USA). After incubation with 100 μL staining solution for 15 min at room temperature, the cells were incubated with 1 mL HEPES (Thermo Fisher Scientific). Apoptosis was detected by flow cytometry with an excitation wavelength of 488 nm.

Chromatin immunoprecipitation (ChIP)

ChIP assays were performed using the ChIP kit (P2078, Beyotime Biotechnology, Shanghai, China) according to the manufacturer's instructions. After the cells were sonicated, the insoluble precipitate was removed by centrifugation at 12,000 × g for 10 min at 4°C. The cells were incubated with Protein G Agarose for 1 h at 4°C. The supernatant was removed by centrifugation at 5,000 × g for 1 min, and 10 μL (1%) of the supernatant was taken out as "Input." The remaining supernatant was incubated with JMJD3 antibody (#3457, 1:50, Cell Signaling Technologies), H3K27me3 antibody (#9733, 1:50, Cell Signaling Technologies), or negative control rabbit anti-IgG (ab172730, 1:25, Abcam) overnight at 4°C. The protein and DNA complexes were precipitated by incubation with protein G Agarose for 1 h at 4°C, and the supernatant was discarded after centrifugation at 5,000 × g for 1 min. The protein and DNA complexes were eluted, de-crosslinked overnight at 65°C, and the DNA fragments were purified and recovered. The purified DNA fragments were used as amplification templates for qPCR experiments to detect the DLX2 promoter expression.

Data analysis

All statistical procedures were carried out using the SPSS 21.0 software (IBM Corp., Armonk, NY, USA). The measurement data were expressed as the mean ± SD and performed at least three experiments. The unpaired t-test was performed for comparisons between any two groups. One-way or two-way ANOVA was used for comparisons among multiple groups, and Tukey's post hoc test was applied for pairwise comparisons. The criterion for statistical significance was taken as $p < 0.05$.

Results

DLX2 is highly expressed in patients with intracranial aneurysm

Differentially expressed genes were analyzed using 2 cases of intracranial aneurysm tissue and 3 cases of intracranial artery tissue from the GEO dataset GSE6551 and annotated through the GPL570 platform (Fig. 1A, B). Three differentially expressed genes were screened by setting the condition logFC > 3: GFAP, DLX2, and ERO1-like protein alpha (Fig. 1C). To investigate the difference in DLX2 expression in the intracranial aneurysm, we detected DLX2 mRNA and protein expression by RT-qPCR and western blot in intracranial aneurysm tissues as well as normal intracranial artery tissues and found that DLX2 was highly expressed in intracranial aneurysm tissues (Fig. 1D, E).

Silencing of DLX2 inhibits proliferation and promotes apoptosis of HA-VSMC

To investigate the effect of DLX2 on the biological activity of HA-VSMC, three shRNAs were selected for DLX2 silencing treatment, and the silencing efficiency was detected by RT-qPCR. All three sh-DLX2 effectively inhibited the expression of DLX2, and sh-DLX2-3 had the best inhibitory effect and was selected for the following experiments (Fig. 2A). The cell proliferation and apoptosis of HA-VMSC were detected by EdU and flow cytometry, which showed that silencing of DLX2 inhibited the proliferation of HA-VMSC and promoted their apoptosis (Fig. 2B, C). Western blot was then conducted to detect the expression of COL1A1, COL3A1, MMP2, and MMP9, and the results showed that silencing of DLX2 promoted the expression of COL1A1 and COL3A1 and inhibited the expression of MMP2 and MMP9 (Fig. 2D).

JMJD3 regulates DLX2 expression through H3K27me3 modification

The expression of JMJD3 in intracranial aneurysm tissues as well as in normal intracranial artery tissues was detected by western blot, and the results showed that JMJD3 was highly expressed in intracranial aneurysm tissues (Fig. 3A). Analysis by the University of California Santa Cruz (UCSC) database (http://genome.ucsc.edu/cgi-bin/hgGateway?hgsid=1269009245_6k6N07YA0wM2Apa sc6Rn1RIpdJd2) revealed that JMJD3 and H3K27me3 had a significant binding relationship near the DLX2 promoter (Fig. 3B, C).
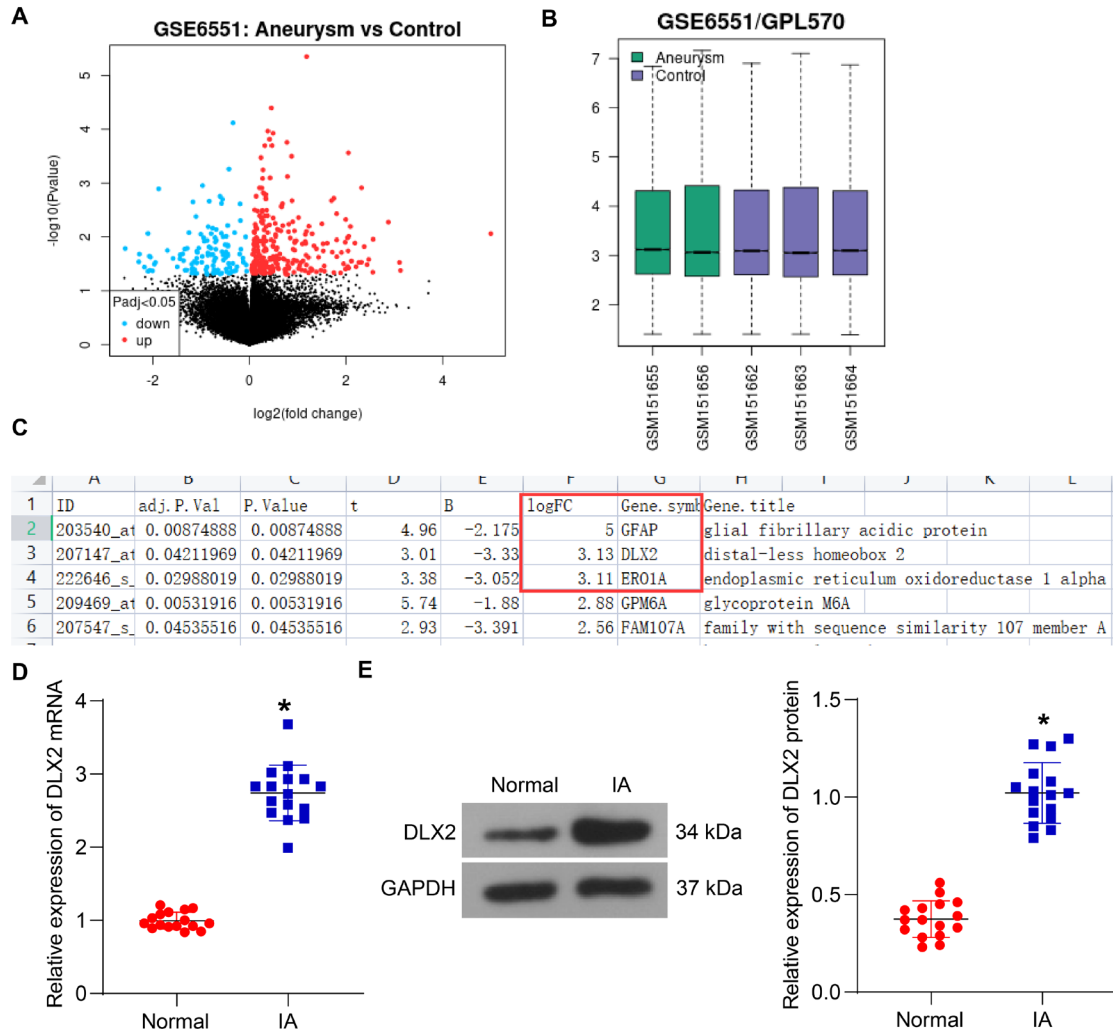
Fig. 1. DLX2 is highly expressed in patients with intracranial aneurysm. (A) Screening for differentially expressed genes in the GSE6551 dataset. (B) Grouping of the sample. (C) Screening of the study subjects. (D) Detection of DLX2 mRNA expression in 16 intracranial aneurysm (IA) tissues and normal intracranial artery tissues by RT-qPCR. (E) Detection of DLX2 protein expression in 16 IA tissues and normal intracranial artery tissues by western blot. $^*p < 0.05$ vs. the normal tissues. The measurement data were expressed as mean ± SD, and the unpaired t-test was performed for comparisons between the two groups.

To further verify the binding relationship between JMJD3 and DLX2 promoter, we conducted a ChIP-qPCR assay. The results showed that the DLX2 promoter fragment was significantly enriched by JMJD3 and H3K27me3 antibodies in HA-VMSC compared with the IgG antibody (Fig. 3D), indicating that both JMJD3 and H3K27me3 could bind the DLX2 promoter. Then, three shRNAs were selected for JMJD3 silencing treatment on HA-VMSC, and the silencing efficiency was detected by RT-qPCR. All three sh-JMJD3 could effectively inhibit the expression of JMJD3, with sh-JMJD3-1 having the best inhibitory effect, so it was selected for the following experiment (Fig. 3E). Western blot was then conducted to detect the expression of DLX2 in HA-VMSC after silencing of JMJD3. The protein expression of DLX2 was also significantly decreased upon JMJD3 knockdown (Fig. 3F). ChIP-qPCR experiments in JMJD3-silenced HA-VMSC (Fig. 3G) showed that the knockdown of JMJD3 resulted in a significant decrease in the enrichment of the DLX2 promoter region by JMJD3 antibody and a significant increase in the enrichment of the DLX2 promoter by H3K27me3 antibody.

JMJD3 modulates the biological activities of HA-VMSC by regulating DLX2 expression

To investigate whether JMJD3 promotes DLX2 expression by inhibiting H3K27me3 modification, thereby affecting HA-VMSC proliferation and apoptosis, we silenced JMJD3 in HA-VMSC or in combination with DLX2 overexpression. The expression of JMJD3, DLX2, COL1A1, COL3A1, MMP2, and MMP9 in HA-VMSC after transfection was detected by western blot. Silencing of JMJD3 significantly decreased the protein expression of
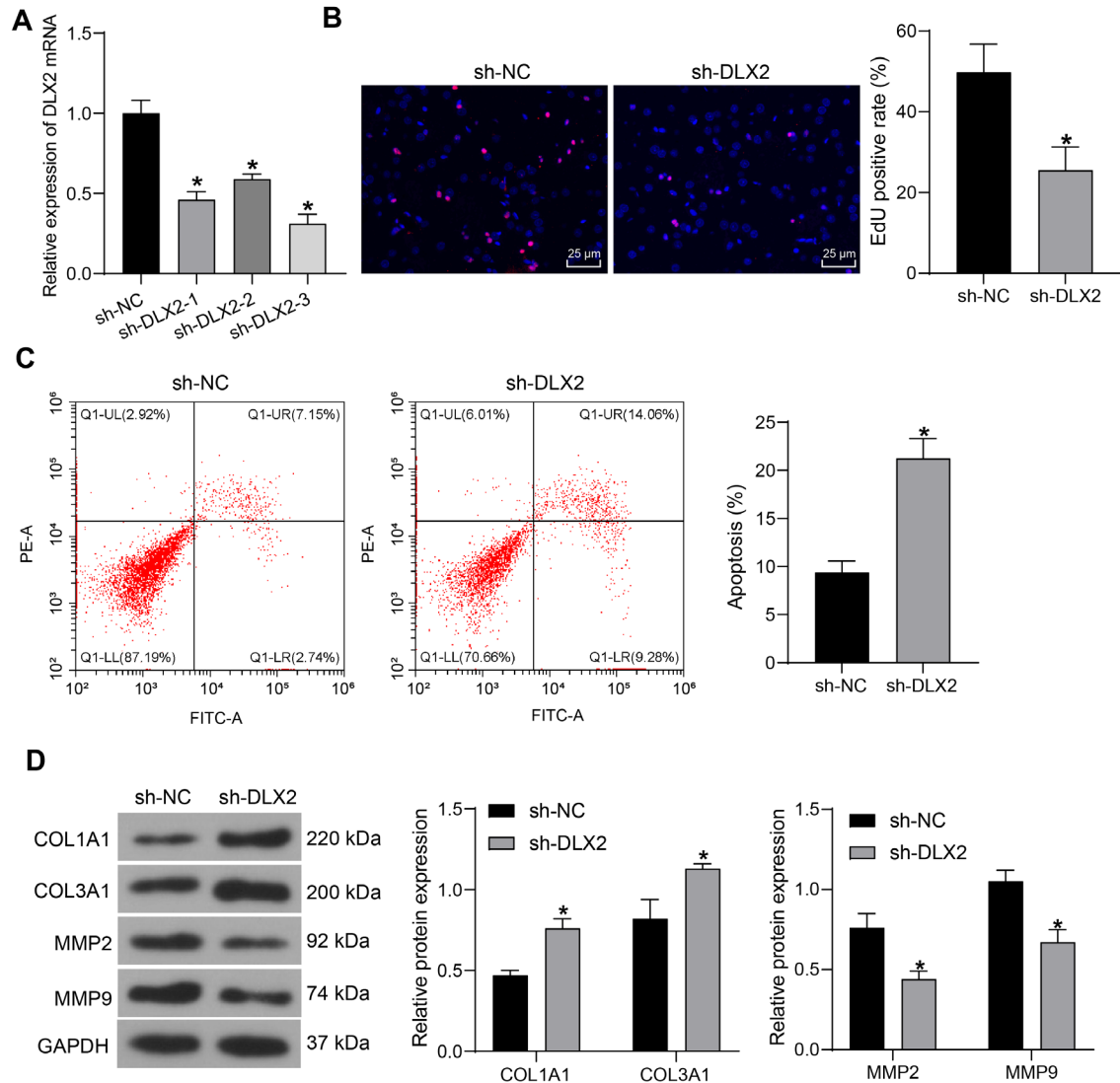
Fig. 2. Silencing of DLX2 governs the proliferation and apoptosis of HA-VSMC.
(A) The silencing efficiency of shRNAs targeting DLX2 by RT-qPCR (n = 3). (B) The proliferation of HA-VSMC was examined using EdU (n = 3). (C) Detection of apoptosis of HA-VSMC by flow cytometry (n = 3). (D) Detection of COL1A1, COL3A1, MMP2 and MMP9 in HA-VSMC by western blot (n = 3). $^*p < 0.05$ vs. the sh-NC group. The measurement data were expressed as mean ± SD. Unpaired *t*-test was performed for comparisons between two groups, one-way or two-way ANOVA was used for comparisons among multiple groups, and Tukey's post hoc test was applied for pairwise comparisons. sh-NC, short hairpin RNA (shRNA) targeting negative control; sh-DLX2, short hairpin RNA (shRNA) targeting DLX2.

DLX2, MMP2, and MMP9, whereas it increased the expression of COL1A1 and COL3A1. Overexpression of DLX2 reversed the effects of sh-JMJD3 on the expression of these proteins (Fig. 4A). Furthermore, silencing of JMJD3 inhibited HA-VMSC proliferation and promoted apoptosis, whereas overexpression of DLX2 reversed the anti-proliferative and pro-apoptotic effects of sh-JMJD3 (Fig. 4B, C).

JMJD3 regulates DLX2 expression in rats with intracranial aneurysm

To perform *in vivo* experiments, rats with intracranial aneurysm were generated, followed by injections of lentivi-

ruses containing sh-JMJD3, sh-DLX2, or sh-JMJD3 + oe-DLX2, and the expression of JMJD3, DLX2, COL1A1, and COL3A1 was detected in arteries of rats using western blot. The expression of JMJD3 and DLX2 was significantly increased, and the expression of COL1A1 and COL3A1 was significantly decreased in the arteries of rats in the Model group (successfully modeled intracranial aneurysm rats) relative to the sham-operated rats. DLX2 was reduced in arteries of rats with intracranial aneurysm after silencing of JMJD3, while JMJD3 expression showed insignificant change upon depletion of DLX2. Loss of JMJD3 and DLX2 showed the same stimulating effects on COL1A1 and COL3A1 expression in intracranial aneurysm rats rela-
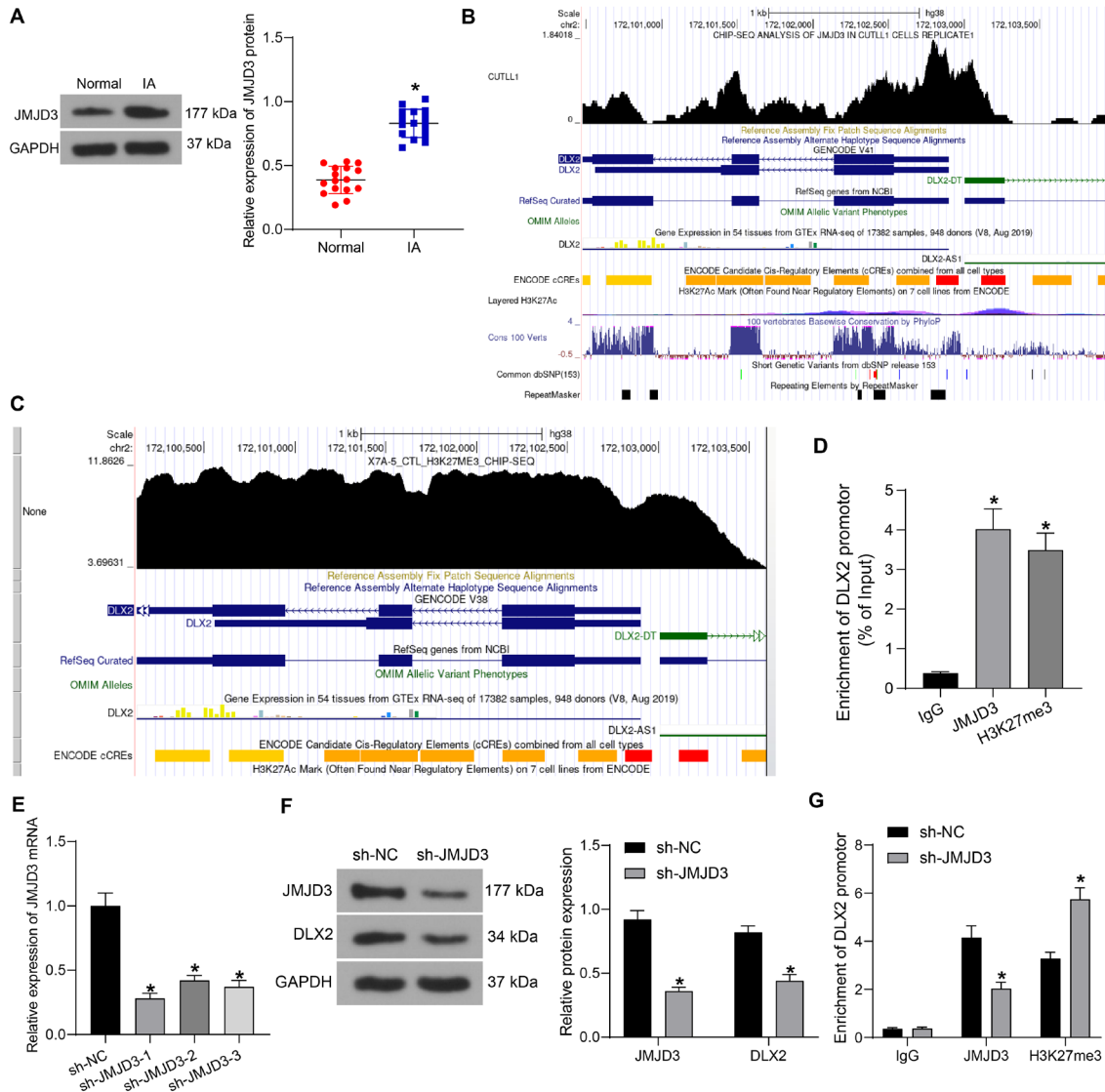
Fig. 3. JMJD3 promotes DLX2 expression through inhibition of H3K27me3 modification.
(A) JMJD3 protein expression in 16 intracranial aneurysm (IA) tissues as well as in normal intracranial artery tissues. (B) The binding relation between JMJD3 and DLX2 was predicted using the UCSC database. (C) The binding relation between H3K27me3 and DLX2 was predicted using the UCSC database. (D) The content of the DLX2 promoter fragment enriched by JMJD3 and H3K27me3 antibody was analyzed using ChIP-qPCR (n = 3). (E) The silencing efficiency of sh-JMJD3 was measured using RT-qPCR (n = 3). (F) JMJD3 and DLX2 protein expression in HA-VSMC after silencing of JMJD3 measured using western blot (n = 3). (G) The content of DLX2 promoter fragment enriched by JMJD3 and H3K27me3 antibody in HA-VSMC after silencing of JMJD3 using ChIP-qPCR (n = 3). $^*p < 0.05$ vs. the IgG group or the sh-NC group. The measurement data were expressed as mean ± SD. Unpaired t-test was performed for comparisons between two groups, one-way or two-way ANOVA was used for comparisons among multiple groups, and Tukey's post hoc test was used for pairwise comparisons.

tive to the sh-NC group. In contrast, DLX2 overexpression reversed the decreasing effect of JMJD3 silencing on DLX2 protein and the promoting effects on COL1A1 and COL3A1 expression in arteries of rats with intracranial aneurysm (Fig. 5A).

Blood pressure measurements were performed in rats, and the results showed that blood pressure increased significantly in the rats with intracranial aneurysm relative to sham-operated rats at 7 and 28 days. The blood pressure was decreased in rats with JMJD3 or DLX2 knockdown

relative to the sh-NC group. DLX2 overexpression reversed the lowering effect of JMJD3 silencing on blood pressure in rats with intracranial aneurysm (Fig. 5B).

Histopathological changes and fibrosis of arteries in rats with intracranial aneurysm were detected by HE staining. The outer membrane and SMCs of the intracranial arteries in the sham group did not show any obvious damage. Intracranial vascular intima injury and increased inflammatory cells were observed in the rats with intracranial aneurysm. Silencing of JMJD3 or DLX2 led to
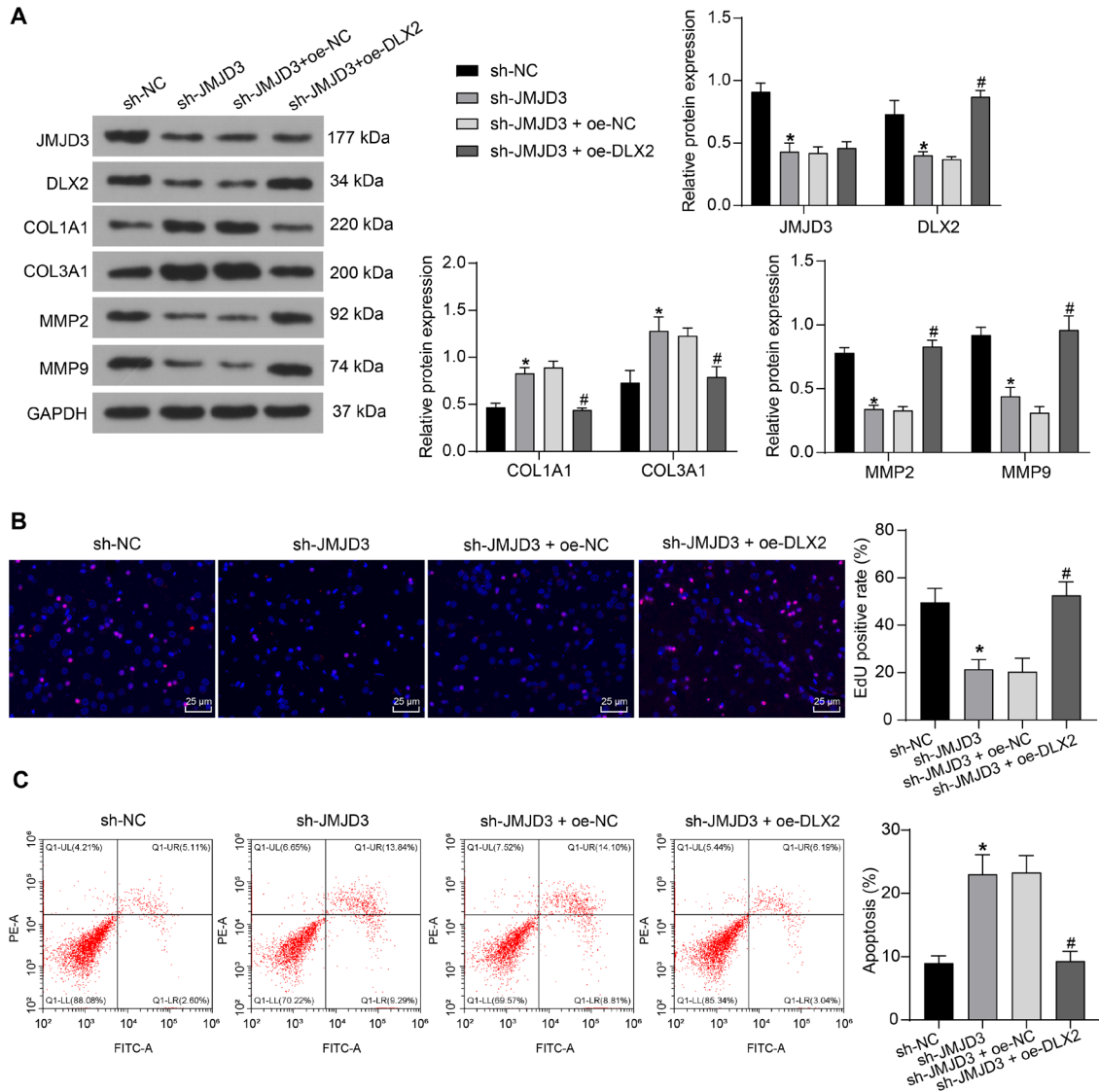
Fig. 4. JMJD3 regulates DLX2 to promote cell proliferation and inhibit apoptosis in HA-VSMC through inhibition of H3K27me3 modification.
HA-VSMC were transfected with sh-JMJD3 alone or with oe-DLX2. (A) Detection of JMJD3, DLX2, COL1A1, CO-L3A1, MMP2 and MMP9 in HA-VSMC by western blot (n = 3). (B) The proliferation of HA-VSMC was examined using EdU (n = 3). (C) Detection of apoptosis of HA-VSMC by flow cytometry (n = 3). $^*p < 0.05$ vs. the sh-NC group; $^#p < 0.05$ vs. the sh-JMJD3 + oe-NC group. The measurement data were expressed as mean ± SD. One-way or two-way ANOVA was used for comparisons among multiple groups and Tukey's post hoc test was applied for pairwise comparisons.

improvement in intracranial arteries of rats with intracranial aneurysm. DLX2 overexpression reversed the ameliorative effect of JMJD3 silencing on intracranial arterial vascular injury in rats with intracranial aneurysm (Fig. 5C). ELISA was conducted to measure the levels of pro-inflammatory factors TNF-α, IL-1β and IL-6 in the tail vein blood of rats. As expected, the levels of these pro-inflammatory factor levels were significantly increased in rats with intracranial aneurysm compared with sham-operated rats. Silencing of JMJD3 or DLX2 significantly reduced the levels of TNF-α, IL-1β, and IL-6 in the tail vein blood of rats with intracranial aneurysm, whereas overexpression of DLX2 reversed the effect of JMJD3 silencing on the reduction of

TNF-α, IL-1β and IL-6 levels (Fig. 5D).

Discussion

Intracranial aneurysm lingers as a possibly devastating disorder, and our understanding of the mechanisms contributing to aneurysm development, progression, and rupture remain incompletely defined (Chalouhi et al. 2012). The phenotypic modulation of SMC in the cerebral circulation or pathogenesis of intracranial aneurysm has been highlighted (Ali et al. 2013; Jiang et al. 2021). In response to vessel injury, SMC undergo phenotypic modulation, a process characterized by increased proliferation, migration, and matrix synthesis (Mack 2011). In our study, we
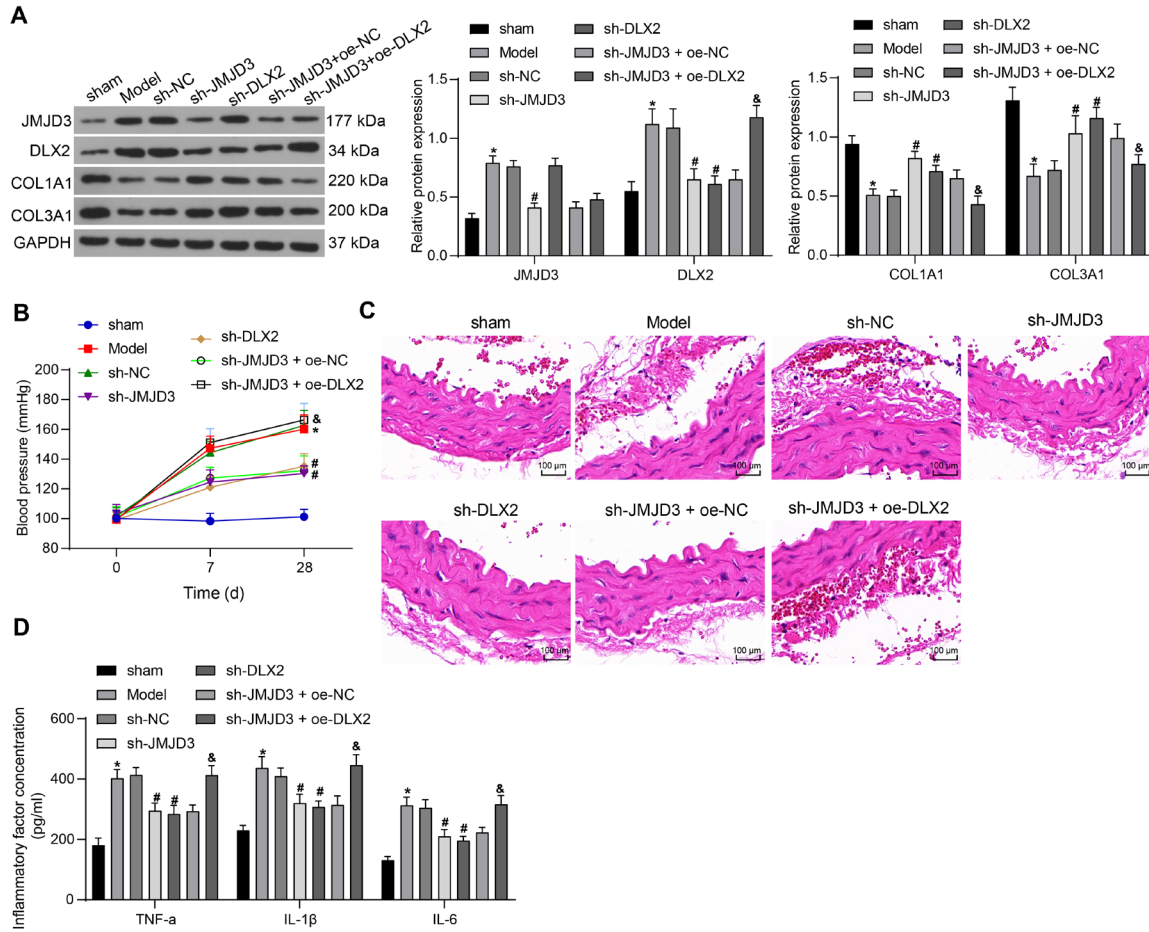
Fig. 5. Silencing of JMJD3 inhibits the formation of intracranial aneurysm.
Rats with intracranial aneurysm were administered with sh-DLX2 or sh-JMJD3 alone, or with oe-DLX2. Model, successfully modeled intracranial aneurysm rats. (A) Detection of COL1A1, COL3A1, DLX2, and JMJD3 in the artery of intracranial aneurysm rat by western blot (n = 8). (B) The blood pressure of rats in each group (n = 8). (C) Histopathological changes of arteries in rats with intracranial aneurysm detected by HE staining (n = 8). (D) The levels of inflammatory factors TNF-α, IL-1β, and IL-6 in the tail vein blood of rats by ELISA (n = 8). $^*p < 0.05$ vs. the sham group; $^\#p < 0.05$ vs. the sh-NC group; $^\&p < 0.05$ vs. the sh-JMJD3 + oe-NC group. The measurement data were expressed as mean ± standard deviation. Two-way ANOVA was used for comparisons among multiple groups and Tukey's post hoc test was used for pairwise comparisons.
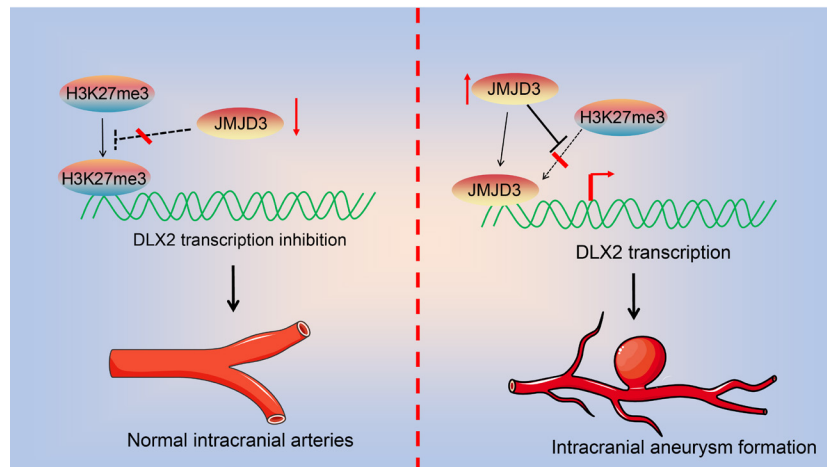

Fig. 6. Proposed mechanism through which JMJD3/DLX2 promotes intracranial aneurysm formation.
Aberrant high expression of JMJD3 promotes transcriptional expression of DLX2 by repressing H3K27me3 modification on the DLX2 promoter, which leads to intracranial aneurysm formation.

revealed that depletion of DLX2 and JMJD3 prevented the proliferation of HA-VSMC. We established a rat model of intracranial aneurysm and found decreases in DLX2 and JMJD3 expression significantly alleviated blood pressure elevation, pro-inflammatory phenotype, and arterial histo-pathological changes in rats. Depletion of JMJD3 was found to be a major target in the regulation of intracranial aneurysm by repressing DLX2 and represents a promising direction in the search for new therapeutic targets in intracranial aneurysm.

DLX2 has been revealed as an oncogene in lung cancer (Park et al. 2021) and hepatocellular carcinoma (Liu et al. 2016; Dai et al. 2020). Moreover, *DLX2* showed a very high level of expression during capillary tube formation (Goyal and Goyal 2019). After identification of overexpression of DLX2 in intracranial aneurysm, we knocked down its expression in HA-VSMC using shRNA. Intracranial aneurysm exhibits loss of the internal elastic lamina, atrophy of the media, and abnormal patterns of extracellular matrix (ECM) expression, during which MMPs are molecules of particular interest because of their upregulation in inflammatory states and their intrinsic ability to degrade ECM components and their role as the main effector molecules in ECM remodeling (Zhang et al. 2019a). Moreover, the formation and progression of intracranial aneurysm are associated with tissue remodeling by the destruction of structural and cellular components, which is related to chronic inflammation (Hosaka and Hoh 2014). In the present study, we found that the depletion of DLX2 significantly reduced the expression of COL1A1, COL3A1, MMP2, and MMP9. In addition, *DLX2* enhanced the proliferative response of neuronal progenitors to epidermal growth factor which is an important factor in mediating ischemia-induced neurogenesis (Zhang et al. 2011). Here, we also observed that silencing of DLX2 reduced the proliferation of HA-VSMC, and restored the apoptosis.

To dissect the upstream modifier for the DLX2 upregulation in intracranial aneurysm, we conducted a literature review. It was reported by Park et al. (2014) that JMJD3 localized at neural enhancers genome-wide in the embryonic brain, and in subventricular zone neural stem cells and regulated the I12b enhancer of DLX2. Consistently, we predicted the binding relation between DLX2 and JMJD3 or H3K27me3. Further, ChIP-PCR validated the regulatory effects of JMJD3/H3K27me3 on DLX2 in HA-VSMC. JMJD3, specifically H3K27me2/3, has been widely studied in immune diseases, cancers, developmental diseases, and aging related diseases (Zhang et al. 2019b). Interestingly, platelet-derived growth factor (PDGF)-BB markedly increased the H3K27me3 level in HA-VSMC, and inhibiting H3K27me3 by treatment with 3-μM UNC1999, an EZH2/1 inhibitor, significantly suppressed PDGF-BB-induced HA-VSMC proliferation (Liang et al. 2019). Inhibition or knockdown of JMJD3 attenuated doxorubicin-induced cardiomyocyte apoptosis, mitochondrial injury, and cardiac dysfunction, whereas JMJD3 overexpression aggra-

vated doxorubicin-induced cardiomyopathy (Wang et al. 2020). JMJD3 was induced in the blood vessels and infiltrated macrophages in a rat model of neuropathic pain, and the JMJD3 demethylase inhibitor GSK-J4 also inhibited the expression and activation of MMP-2 and MMP-9 and significantly alleviated the loss of tight junction proteins (Lee et al. 2021). The suppressing effects of JMJD3 inhibition on MMP-2 and MMP-9 expression were also validated in brain microvascular endothelial cells subjected to TNF-α treatment (Na et al. 2017). Indirect evidence has also been given that lanthanum chloride inhibited proinflammatory cytokine and adhesion molecule expressions induced by lipopolysaccharides in human umbilical vein endothelial cells (Chen et al. 2017). Also, JMJD3 silencing or the administration of the JMJD3 inhibitor GSK-J4 significantly decreased the inflammatory response in IL-1β-treated synovial fibroblasts, mainly by controlling the methylation status of H3K27me3 at the promoter of its target genes (Wu et al. 2019). However, there is little information regarding the regulatory role of JMJD3 on the HA-VSMC. Our data presented that the loss of JMJD3 reduced the expression of MMP2 and MMP9 and the proliferation of HA-VSMC, which was reversed by DLX2 overexpression.

In summary, our study has revealed that DLX2 and JMJD3 expression was upregulated in intracranial aneurysm patients compared to normal tissues. JMJD3 expedited proinflammatory cytokine production, including IL-1β, IL-6, and TNF-α, and the viability of HA-VSMC by enhancing the expression of DLX2, along with upregulated expression of MMP2 and MMP9 (Fig. 6). Taken together, our study has indicated that the JMJD3/DLX2 axis has an important role in intracranial aneurysm formation.

Acknowledgments

Conflict of Interest

The authors declare no conflict of interest.

References

Ali, M.S., Starke, R.M., Jabbour, P.M., Tjoumakaris, S.I., Gonzalez, L.F., Rosenwasser, R.H., Owens, G.K., Koch, W.J., Greig, N.H. & Dumont, A.S. (2013) TNF-α induces phenotypic modulation in cerebral vascular smooth muscle cells: implications for cerebral aneurysm pathology. *J. Cereb. Blood Flow Metab.*, **33**, 1564-1573.

Cai, Y., Huang, D., Ma, W., Wang, M., Qin, Q., Jiang, Z. & Liu, M. (2021) Histone deacetylase 9 inhibition upregulates microRNA-92a to repress the progression of intracranial aneurysm via silencing Bcl-2-like protein 11. *J. Drug Target.*, **29**, 761-770.

Chalouhi, N., Ali, M.S., Jabbour, P.M., Tjoumakaris, S.I., Gonzalez, L.F., Rosenwasser, R.H., Koch, W.J. & Dumont, A.S. (2012) Biology of intracranial aneurysms: role of inflammation. *J. Cereb. Blood Flow Metab.*, **32**, 1659-1676.

Chen, X., Xiu, M., Xing, J., Yu, S., Min, D. & Guo, F. (2017) Lanthanum chloride inhibits LPS mediated expressions of pro-inflammatory cytokines and adhesion molecules in HUVECs:

involvement of NF-κB-Jmjd3 signaling. *Cell. Physiol. Biochem.*, **42**, 1713-1724.

Dai, Q., Deng, J., Zhou, J., Wang, Z., Yuan, X.F., Pan, S. & Zhang, H.B. (2020) Long non-coding RNA TUG1 promotes cell progression in hepatocellular carcinoma via regulating miR-216b-5p/DLX2 axis. *Cancer Cell Int.*, **20**, 8.

Davis, F.M., Tsoi, L.C., Melvin, W.J., denDekker, A., Wasikowski, R., Joshi, A.D., Wolf, S., Obi, A.T., Billi, A.C., Xing, X., Audu, C., Moore, B.B., Kunkel, S.L., Daugherty, A., Lu, H.S., et al. (2021) Inhibition of macrophage histone demethylase JMJD3 protects against abdominal aortic aneurysms. *J. Exp. Med.*, **218**, e20201839.

Goyal, D. & Goyal, R. (2019) Angiogenic transformation in human brain micro endothelial cells: whole genome DNA methylation and transcriptomic analysis. *Front. Physiol.*, **10**, 1502.

Hosaka, K. & Hoh, B.L. (2014) Inflammation and cerebral aneurysms. *Transl. Stroke Res.*, **5**, 190-198.

Jiang, Z., Huang, J., You, L., Zhang, J. & Li, B. (2021) STAT3 contributes to intracranial aneurysm formation and rupture by modulating inflammatory response. *Cell. Mol. Neurobiol.*, **41**, 1715-1725.

Jones, J.A., Barbour, J.R., Stroud, R.E., Bouges, S., Stephens, S.L., Spinale, F.G. & Ikonomidis, J.S. (2008) Altered transforming growth factor-beta signaling in a murine model of thoracic aortic aneurysm. *J. Vasc. Res.*, **45**, 457-468.

Lagunas-Rangel, F.A. (2021) KDM6B (JMJD3) and its dual role in cancer. *Biochimie*, **184**, 63-71.

Lee, J., Choi, H., Park, C., Jeon, S. & Yune, T. (2021) Jmjd3 mediates neuropathic pain by inducing macrophage infiltration and activation in lumbar spinal stenosis animal model. *Int. J. Mol. Sci.*, **22**, 13426.

Li, S.M., He, L.R., Chen, J.W., Zhou, J., Nie, R.C., Jin, X.H., Wang, X., Fu, J.H., Wang, F.W. & Xie, D. (2020) JMJD3 promotes esophageal squamous cell carcinoma pathogenesis through epigenetic regulation of MYC. *Signal Transduct. Target. Ther.*, **5**, 165.

Liang, J., Li, Q., Cai, W., Zhang, X., Yang, B., Li, X., Jiang, S., Tian, S., Zhang, K., Song, H., Ai, D., Zhang, X., Wang, C. & Zhu, Y. (2019) Inhibition of polycomb repressor complex 2 ameliorates neointimal hyperplasia by suppressing trimethylation of H3K27 in vascular smooth muscle cells. *Br. J. Pharmacol.*, **176**, 3206-3219.

Liu, J., Cui, X., Qu, L., Hua, L., Wu, M., Shen, Z., Lu, C. & Ni, R. (2016) Overexpression of DLX2 is associated with poor prognosis and sorafenib resistance in hepatocellular carcinoma. *Exp. Mol. Pathol.*, **101**, 58-65.

Liu, Z., Ajimu, K., Yalikun, N., Zheng, Y. & Xu, F. (2019) Potential therapeutic strategies for intracranial aneurysms targeting aneurysm pathogenesis. *Front. Neurosci.*, **13**, 1238.

Mack, C.P. (2011) Signaling mechanisms that regulate smooth muscle cell differentiation. *Arterioscler. Thromb. Vasc. Biol.*, **31**, 1495-1505.

Na, W., Shin, J.Y., Lee, J.Y., Jeong, S., Kim, W.S., Yune, T.Y. & Ju, B.G. (2017) Dexamethasone suppresses JMJD3 gene activation via a putative negative glucocorticoid response element

and maintains integrity of tight junctions in brain microvascular endothelial cells. *J. Cereb. Blood Flow Metab.*, **37**, 3695-3708.

Park, D.H., Hong, S.J., Salinas, R.D., Liu, S.J., Sun, S.W., Sgualdino, J., Testa, G., Matzuk, M.M., Iwamori, N. & Lim, D.A. (2014) Activation of neuronal gene expression by the JMJD3 demethylase is required for postnatal and adult brain neurogenesis. *Cell Rep.*, **8**, 1290-1299.

Park, H.R., Choi, Y.J., Kim, J.Y., Kim, I.G. & Jung, U. (2021) Repeated irradiation with γ-ray induces cancer stemness through TGF-β-DLX2 signaling in the A549 human lung cancer cell line. *Int. J. Mol. Sci.*, **22**, 4284.

Poppenberg, K.E., Zebraski, H.R., Avasthi, N., Waqas, M., Siddiqui, A.H., Jarvis, J.N. & Tutino, V.M. (2021) Epigenetic landscapes of intracranial aneurysm risk haplotypes implicate enhancer function of endothelial cells and fibroblasts in dysregulated gene expression. *BMC Med. Genomics*, **14**, 162.

Samuel, N. & Radovanovic, I. (2019) Genetic basis of intracranial aneurysm formation and rupture: clinical implications in the postgenomic era. *Neurosurg. Focus*, **47**, E10.

Sanchez, A., Houfaf Khoufaf, F.Z., Idrissou, M., Penault-Llorca, F., Bignon, Y.J., Guy, L. & Bernard-Gallon, D. (2021) The functions of the demethylase JMJD3 in cancer. *Int. J. Mol. Sci.*, **22**, 968.

Starke, R.M., Chalouhi, N., Ding, D., Raper, D.M., McKisic, M.S., Owens, G.K., Hasan, D.M., Medel, R. & Dumont, A.S. (2014) Vascular smooth muscle cells in cerebral aneurysm pathogenesis. *Transl. Stroke Res.*, **5**, 338-346.

Tan, Y. & Testa, J.R. (2021) DLX genes: roles in development and cancer. *Cancers* (*Basel*), **13**, 3005.

Tromp, G., Weinsheimer, S., Ronkainen, A. & Kuivaniemi, H. (2014) Molecular basis and genetic predisposition to intracranial aneurysm. *Ann. Med.*, **46**, 597-606.

Wang, P., Lan, R., Guo, Z., Cai, S., Wang, J., Wang, Q., Li, Z., Li, Z., Wang, Q., Li, J., Wu, Z., Lu, J. & Liu, P. (2020) Histone demethylase JMJD3 mediated doxorubicin-induced cardiomyopathy by suppressing SESN2 expression. *Front. Cell Dev. Biol.*, **8**, 548605.

Wu, W., Qin, M., Jia, W., Huang, Z., Li, Z., Yang, D., Huang, M., Xiao, C., Long, F., Mao, J., Moore, P.K., Liu, X. & Zhu, Y.Z. (2019) Cystathionine-γ-lyase ameliorates the histone demethylase JMJD3-mediated autoimmune response in rheumatoid arthritis. *Cell. Mol. Immunol.*, **16**, 694-705.

Zhang, C., Wu, H., Zhu, X., Wang, Y. & Guo, J. (2011) Role of transcription factors in neurogenesis after cerebral ischemia. *Rev. Neurosci.*, **22**, 457-465.

Zhang, X., Ares, W.J., Taussky, P., Ducruet, A.F. & Grandhi, R. (2019a) Role of matrix metalloproteinases in the pathogenesis of intracranial aneurysms. *Neurosurg. Focus*, **47**, E4.

Zhang, X., Liu, L., Yuan, X., Wei, Y. & Wei, X. (2019b) JMJD3 in the regulation of human diseases. *Protein Cell*, **10**, 864-882.

Zurek, M., Aavik, E., Mallick, R. & Yla-Herttuala, S. (2021) Epigenetic regulation of vascular smooth muscle cell phenotype switching in atherosclerotic artery remodeling: a mini-review. *Front. Genet.*, **12**, 719456.